A Wavelet Packet Transform Inspired Method of Neutron-Gamma Discrimination

David I. Shippen, Malcolm J. Joyce, and Michael D. Aspinall

***Abstract*—A Simplified Digital Charge Collection (SDCC) method of discrimination between neutron and gamma pulses in an organic scintillator is presented and compared to the Pulse Gradient Analysis (PGA) discrimination method. Data used in this research were gathered from events arising from the $^7\mathrm{Li(p,n)}^7\mathrm{Be}$ reaction detected by an EJ-301 organic liquid scintillator recorded with a fast digital oscilloscope. Time-of-Flight (TOF) data were also recorded and used as a second means of identification. The SDCC method is found to improve on the figure of merit (FOM) given by PGA method at the equivalent sampling rate.**

***Index Terms*—Digital, liquid scintillators, pulse-shape discrimination, time of flight.**

I. Introduction

NEUTRONS with energies in excess of 0.5 MeV are often detected with the use of an organic scintillator. These detectors have the advantages of portability, chemical stability and affordability in applications found in industry, medicine and homeland security. Scintillation compounds with reduced flammability have been developed in recent years which make the application of these detectors even more attractive [1]. The majority of this group of scintillation materials responds to both the neutron and the photon component of a mixed radiation field. It has long been documented that the discrimination of these neutron and photon interactions in an organic scintillator is achieved by inspecting the pulse shape that results [2]. The decay length of the trailing edge of the pulse has been modeled mathematically by Marrone *et al.* and this model reflects the well-known property that it takes longer for the neutron interaction to decay than a gamma-ray interaction [2], [3].

All neutron fields coexist with an associated gamma-ray component resulting from the scattering reactions of the neutrons with materials in the environment and as direct by-products of the primary reaction producing the neutron field. Hence, pulse shape discrimination is essential in fast neutron spectrometry with organic liquid scintillators.

It is only recently that digital electronics have been capable of the processing speeds required to capture and process scintillator pulses. Beforehand, analogue electronic modules were used which were often temperamental to set up and not compatible with modern computerised data acquisition systems.

Embedded systems with analogue-to-digital converters (ADC) with sampling rates of 500 $\mathrm{MSa \cdot s^{-1}}$ are now commonplace in industry at an affordable cost. With the advent of these new technologies fast, digital methods of pulse-shape discrimination have evolved.

Pulse Gradient Analysis (PGA), a fast digital discrimination technique developed at the Lancaster University Engineering Department, has been reported [4] and has been verified successfully using time-of-flight (TOF) data [1]. This paper details an attempt to further optimize digital methods of pulse shape discrimination for use on embedded platforms.

II. Experimental

The data for this research were generated at the National Physical Laboratory (NPL) Neutron Irradiation Facility located in Teddington, UK. The NPL Van de Graaff accelerator was employed to produce a 2.924 MeV proton beam which was incident on a thin 60 $\mu\mathrm{g \cdot cm^{-2}}$ lithium fluoride target. Via the $^7\mathrm{Li(p,n)}^7\mathrm{Be}$ reaction, neutrons with energies of 1.225 MeV and 0.745 MeV were produced corresponding to transitions to the ground and first excited states, respectively, of the product nucleus. The accelerator was operated in pulse mode and a capacitive-type detector was placed in the beam 1.6 m from the lithium fluoride target to detect the arrival of the proton beam pulse as it strikes the target. This arrangement provides timing information on the beam-pickup signal which is used to determine the TOF measurement and information on the proton pulse duration and frequency. The transit time from the pickup to the target is constant because the proton beam is mono-energetic and the target is very thin. Therefore, there is a constant delay between the beam-pickup signal and the emission of neutrons from the $^7\mathrm{Li(p,n)}^7\mathrm{Be}$ reaction. Thus, the beam pickup is used to identify the start, pulse duration and period of the subsequent neutron pulses. The proton pulse in this experiment had a period of 400 ns and a pulsewidth of 5 ns. No attempt was made to account for scatter of neutrons into the detector using shadow-cone measurements although such a contribution was anticipated to be small. The experiment is shown diagrammatically in Fig. 1.

The experimental setup for this research used a 4.5 ml scintillation cell filled with EJ-301 organic liquid (John Caunt Scientific Ltd., UK), optically-coupled to a Hamamatsu R5611 photomultiplier tube (PMT). The PMT was operated with a negative high-tension (HT) supply voltage of -840 V DC. The output signal from the scintillator was connected to channel 1 of an Infiniium® digital oscilloscope (Agilent Tech.), via approximately 30 m of high-bandwidth cable (Huber + Suhner

Manuscript received June 12, 2009; revised December 31, 2009; accepted February 15, 2010. Date of current version October 15, 2010. The work of M.D. Aspinall was supported in part by the Ministry of Defense (MoD) and the Engineering and Physical Sciences Research Council (EPSRC).

The authors are with the Engineering Department, Lancaster University, Lancaster LA1 4YR, U.K. (e-mail: m.joyce@lancaster.ac.uk; m.aspinall@lancaster.ac.uk).

Color versions of one or more of the figures in this paper are available online at http://ieeexplore.ieee.org.

Digital Object Identifier 10.1109/TNS.2010.2044190

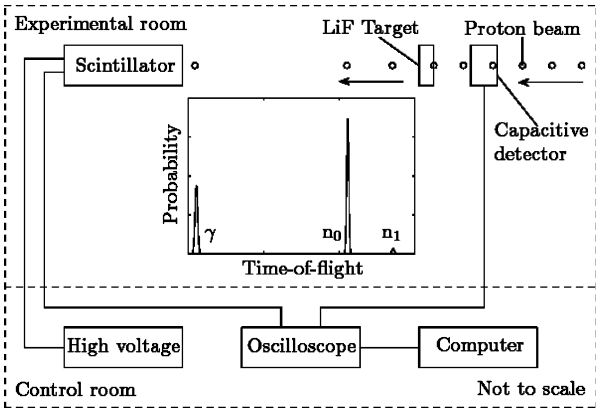

Fig. 1. A schematic diagram of the experimental setup at the Neutron Irradiation Facility, National Physical Laboratory.

SX 07262 BD). This cable preserved the pulse shape sufficiently to allow discrimination methods to be developed, whereas the standard RG58 did not. The beam pick-up signal was connected to a leading-edge discriminator in the control room and the discriminator output was then passed (with a delay) to another input of the digital oscilloscope. The scintillator was positioned 54 mm vertically off axis and 1613 mm horizontally from the face of the lithium fluoride target.

Scintillator pulses were used to trigger acquisition. Acquisition of the scintillator pulse and corresponding beam-pickup pulse data were recorded digitally with a sampling rate of 8 $\mathrm{GSa} \cdot \mathrm{s}^{-1}$ and 16-bit amplitude resolution. The acquisition was automated by driving the oscilloscope remotely via a Transmission Control Protocol/Internet Protocol (TCP/IP) connection to a personal computer running a bespoke MATLAB® program. This enabled all detected events i.e., the 1.225 MeV neutron, the 0.745 MeV neutron, gamma rays and scattered events to be sorted in terms of their time of arrival relative to the initial beam-pickup signal [1].

III. Background

The Fourier Transform method of frequency analysis maps each point of a continuous, piece-wise linear waveform in the time domain to a unique point in the frequency domain. This transform assumes that the signal that is being transformed is static; that is each frequency component is present throughout and all time information is lost. Dynamic signals have frequency components that occur at different times. In the case of an EJ-301 organic liquid scintillator, the amount of delayed fluorescence present in the signal determines whether the interaction within was a light particle or photon or a heavier particle [2].

The Continuous Wavelet Transform (CWT) was conceived to provide both time and frequency information. A mother wavelet is scaled and shifted and then convolved with the target signal. Frequency information is gathered by varying the scale and time information is gathered by varying the shift. Unfortunately, the CWT is unfeasible to implement on an embedded platform due to the large processor and memory overhead needed to perform the calculation [5]. For this reason the CWT has not been pursued further in this research.

The Discrete Wavelet Transform (DWT) is a discretized version of the CWT. The mother wavelet is sampled and each sample from the signal is convolved with the sampled wavelet. It has been shown that passing the signal through a bank of quadrature mirror filters with suitable coefficients is equivalent to the DWT. In this form the Wavelet Transform is well suited to the embedded platform. Digital Signal Processors (DSPs) and Field Programmable Gate Arrays (FPGAs) are well-suited to perform this task quickly and efficiently [6].

When the signal is passed through this bank of filters, the low-pass filter, h, gives the approximation coefficients and the high-pass filter, g, gives the detail coefficients. If the size of the signal is 2^n samples, where n is a positive integer, then the length of the approximation and detail coefficients are both 2^{n-1} due to the Nyquist theorem. The approximation and detail coefficients are down-sampled by two. Time resolution is therefore reduced by a factor of two and frequency resolution is increased by a factor of two. The bank of filters can then be applied again to the approximation coefficients. Again, this halves the time resolution and doubles the frequency resolution. This process can be repeated n times or, in other words, we are able to decompose the signal up to the nth scale [7]. It is advantageous to keep the original signal length as a power of two. Otherwise, a scheme must be used which pads out the signal to a length of the next power of two. Padding has consequences on the frequency spectrum as unwanted artifacts are introduced [8].

The Wavelet Packet Transform (WPT) is an iteration of the quadrature mirror bank implementation of the DWT. Instead of just the approximation coefficients being fed through to the next scale, both the approximation and detail coefficients are passed through the filter bank. This has the effect of decomposing the signal into all possible time-frequency resolutions.

Using the WPT it is possible to visualize how the frequencies of a signal vary with time. Although it is not possible to have maximum time resolution at the same time as maximum frequency resolution, a trade-off can be reached. This trade-off is reached when the time resolution is the same as the frequency resolution. This is equivalent to drawing a horizontal basis across the WPT. For a signal length of 2^n the level basis is at scale $n/2$ when n is even. When n is odd it is not possible to have a frequency resolution the same as the time resolution and in this case one may choose a better frequency resolution by opting to round n down or, if preferred, choose a better time resolution by rounding n up to the nearest integer. Visualization is achieved by plotting a dyadic grid of time-bin against frequency-bin against the square of each coefficient in the WPT after natural frequency ordering [9].

WPT visualization at a basis with equal time and frequency resolution was performed on the pulses given by the scintillator-PMT combination with the Daubechies 4 quadrature mirror filters. No particular frequency or set of frequencies over time were observed that characterized a significant difference between neutron and gamma pulses. To achieve discrimination from the coefficients gained from the WPT it was necessary to sum the squares of the coefficients that corresponded to all frequencies contained in the signal at the latter time of the

pulse. This is equivalent to determining the energy at the tail end of the pulse and is an application of Parseval's equation [10]:

$$\frac{1}{2\pi}\int_0^{2\pi}\left|X(e^{j\omega})\right|^2 d\omega = \sum_{n\in Z}|x[n]|^2, \tag{1}$$

where $x[n]$ denotes the nth sample of the sequence x and $X(\cdot)$ is the representation of x in the frequency domain. This is a digital method of an analogue charge comparison employed in industry for several decades. Thus, the frequency analysis described above was optimized by simply squaring each sample in the time domain that falls in the region of interest of the pulse.

IV. Analytical Considerations

The dataset used in this research is identical to the dataset used recently to verify a method called Pulse Gradient Analysis developed by the Lancaster Engineering Department. Furthermore, the same MATLAB® scripts were used to determine pulse type via the TOF and hence provide a means of segregating the pulses into radiation type. Full details of the TOF method of discrimination can be found in [1] and full details of the PGA discrimination method can be found in [4], [11].

In total 2500 pulses were available for analysis. These pulses were tagged according to radiation type and all were digitally baseline corrected to remove the DC offset present at the output of the scintillator-PMT combination.

A. PGA Method of Pulse-Shape Discrimination

PGA was designed to be a fast and simple method of discrimination between gamma and neutron events in organic liquid scintillators for embedded processors such as FPGAs. In the time domain Marrone mathematically modeled the fact that a light pulse due to a neutron interaction decays more slowly than that for a gamma-ray interaction [3]. The PGA method plots the peak amplitude of the pulse on the ordinate and the amplitude of the pulse at a specified time afterwards, known as the discrimination amplitude, on the abscissa. The resulting scatter diagram produces a discrimination plane which produces two plumes which categorizes the event type.

MATLAB® scripts used in [1] were obtained and used to produce PGA discrimination. These scripts reduced the initial sampling rate of the oscilloscope of 8 $\mathrm{GSa\cdot s^{-1}}$ to 250 $\mathrm{MSa\cdot s^{-1}}$ by discarding the interim data points. The scripts also applied a 21-point, recursive, moving average filter. The discrimination amplitude was set as 20 ns after the peak.

B. Simplified Digital Charge Comparison Method of Pulse-Shape Discrimination

The Simplified Digital Charge Comparison (SDCC) method developed in this research also depends on the decay rate difference of neutron interaction and gamma-ray interaction in organic scintillators. In this method the rise time proportion of the pulse is discarded and the peak of each pulse is considered to be sample number one. Each of the 2500 pulses available in this research were then cropped to have a pulse length of 128 ns which corresponds to having 1024 samples at the original sampling rate of 8 $\mathrm{GSa\cdot s^{-1}}$.

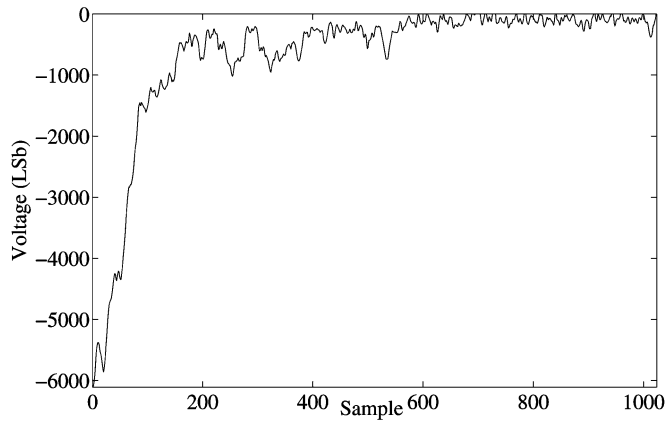

Fig. 2. A typical neutron pulse sampled at 8 $\mathrm{GSa\cdot s^{-1}}$ after baseline correction.

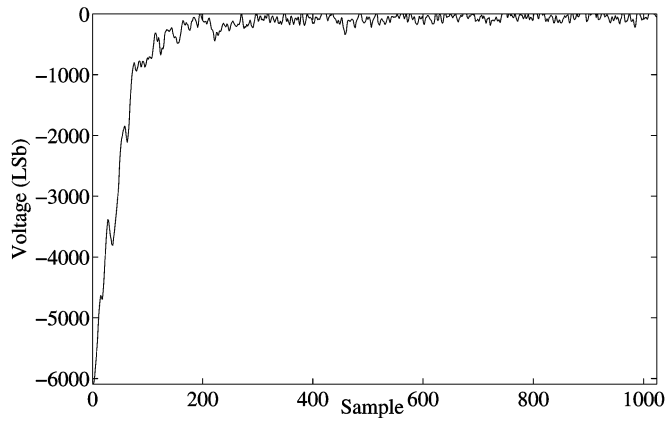

Fig. 3. A typical gamma pulse sampled at 8 $\mathrm{GSa\cdot s^{-1}}$ after baseline correction.

Fig. 2 shows a typical neutron pulse and Fig. 3 shows a typical gamma-ray pulse.

The difference between the neutron and gamma pulse is evident between samples 192 and 512 or between three-sixteenths and one half of the pulse length. This is a clear example of the slower decay rate due to a neutron interaction compared to a gamma-ray interaction.

From this empirical assessment of the difference between pulses the SDCC discrimination parameter, D, is defined to be for each pulse:

$$D = \log\left(\sum_{n=192}^{512} x_n^2\right), \tag{2}$$

where x_n is the magnitude of the nth sample of the pulse. This is a measure of the energy of the signal between three-sixteenths and one half of the pulse length. For lower sampling rates the ranges of the sum are adjusted accordingly. Please note that voltage measurements are kept in Least Significant Bit (LSb) form to remain as optimized as possible for the embedded system format.

The discrimination plane in the SDCC method is plotted with the pulse height on the abscissa and the D parameter on the ordinate since we wish to exploit uncertainty in D to discern the event pulses. Because the D parameter is an accumulative sum of the samples squared then the uncertainties are going to

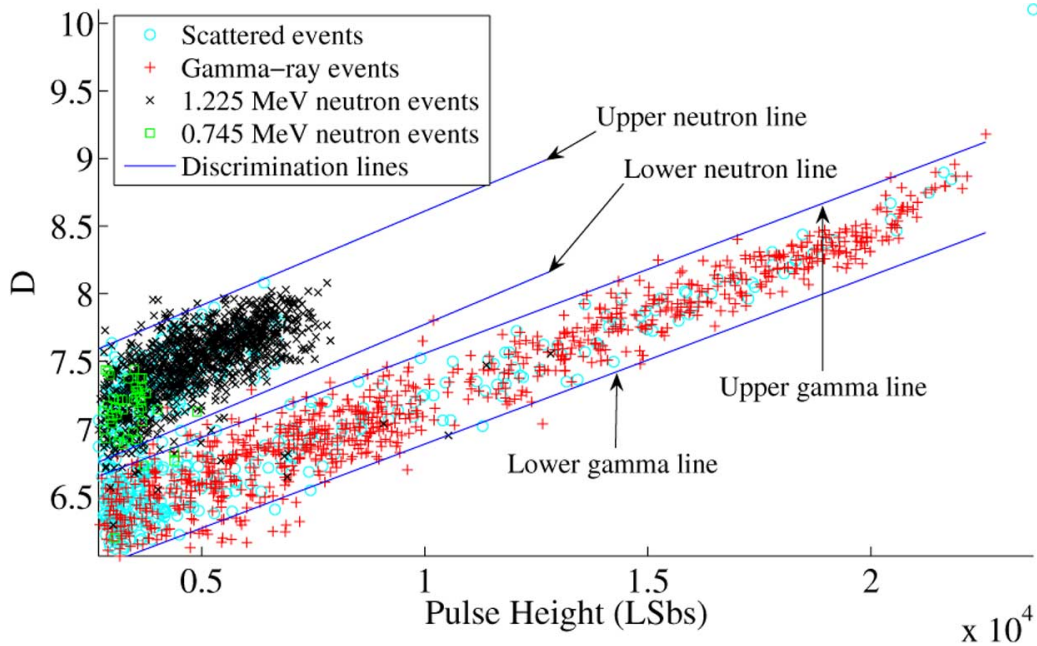

Fig. 4. The SDCC discrimination plane at a sampling rate of 8 $\mathrm{GSa} \cdot \mathrm{s}^{-1}$ together with the tag from the TOF discrimination corresponding to colour as per the legend.

be much larger than they are for the pulse height. For curve fitting, it is best practise to have the variable with the lower uncertainties in the independent variable [12].

C. Figure of Merit

Traditionally, the Figure of Merit (FOM) of a discrimination method has relied upon the calculation of a single figure which is used to identify interaction type by simple bounds checking, e.g., if the discrimination figure is over a certain value then it is a particular interaction type. The normalized probability distribution of the discrimination parameter is then obtained and a double Gaussian distribution fitted to the equation:

$$f(x) = A_1 e^{-\left((x-\mu_1)^2/2\sigma_1^2\right)} + A_2 e^{-\left((x-\mu_2)^2/2\sigma_2^2\right)}. \quad (3)$$

The FOM is then calculated by:

$$FOM = \frac{S}{FWHM_1 + FWHM_2}, \quad (4)$$

where S is the distance of the two means of the double Gaussian fit and $FWHM_1$ and $FWHM_2$ are the Full Width at Half Maximum values of the two peaks of this fit.

The PGA and SDCC methods rely on two parameters for discrimination and hence map points to a plane. Choosing one of these parameters for the FOM calculation will not give a fair representation as the spread of values in a single dimension are likely to overlap, i.e., a value of one parameter will map to several values of the second parameter and vice-versa.

For this research to be compatible with the traditional FOM a straight line has to be fitted on each of the discrimination planes. From this straight line a probability distribution of the distance of each point in the discrimination plane to that line can be taken as a replacement of distribution of a single parameter in the traditional case.

TABLE I
THE RESULTS OF A LINEAR FIT TO THE NEUTRON AND GAMMA PLUMES PRODUCED BY THE SDCC DISCRIMINATION METHOD

Sample rate		Gradient	Offset	σ_{perp}
8 GSa·s^{-1}	Neutron Line	1.39x10^{-4}	6.80	0.214
	Uncertainty	±5.01x10^{-6}	±2.52x10^{-2}	-
	Gamma Line	1.24x10^{-4}	5.98	0.171
	Uncertainty	±1.06x10^{-6}	±1.25x10^{-2}	-
250 MSa·s^{-1}	Neutron Line	1.48x10^{-4}	5.41	0.238
	Uncertainty	±5.58x10^{-6}	±2.81x10^{-2}	-
	Gamma Line	1.37x10^{-4}	4.55	0.216
	Uncertainty	±1.33x10^{-6}	±1.57x10^{-2}	-

V. RESULTS

Fig. 4 shows the discrimination plane of the SDCC method for the 2500 pulses sampled at 8 $\mathrm{GSa} \cdot \mathrm{s}^{-1}$. Each point in the plane has been tagged with the pulse type the TOF has assigned to it. With the TOF data it is possible to mask the data obtained from the SDCC method. With this mask in place standard linear least-squares fitting was performed on the gamma data and again on the 1.225 MeV and 0.745 MeV neutron data combined. The results are presented in Table I.

After the centroid is calculated for each plume the distribution of the points about their relevant fit is calculated. This was done by calculating the perpendicular distance from each point in the discrimination plane to the corresponding straight line fit. The standard deviation was then calculated and is given as σ_{perp} in Table I.

σ_{perp} is used to calculate the discrimination lines presented in Fig. 4. These discrimination lines are the same gradient as the centroid fit but the offset is changed by $\pm 1.96\ \sigma_{perp}$ hence the four discrimination lines drawn in Fig. 4. This is equivalent to bounding each plume with the 95% probability of all the points that lie inside those bounds, assuming a Gaussian distribution.

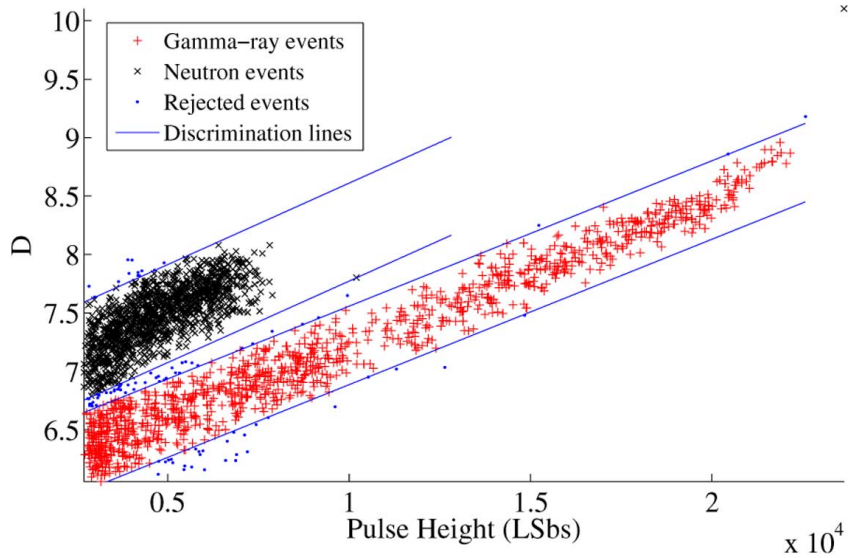

Fig. 5. The SDCC discrimination plane at a sampling rate of 8 $\mathrm{GSa} \cdot \mathrm{s}^{-1}$ with the boundary method of pulse categorization.

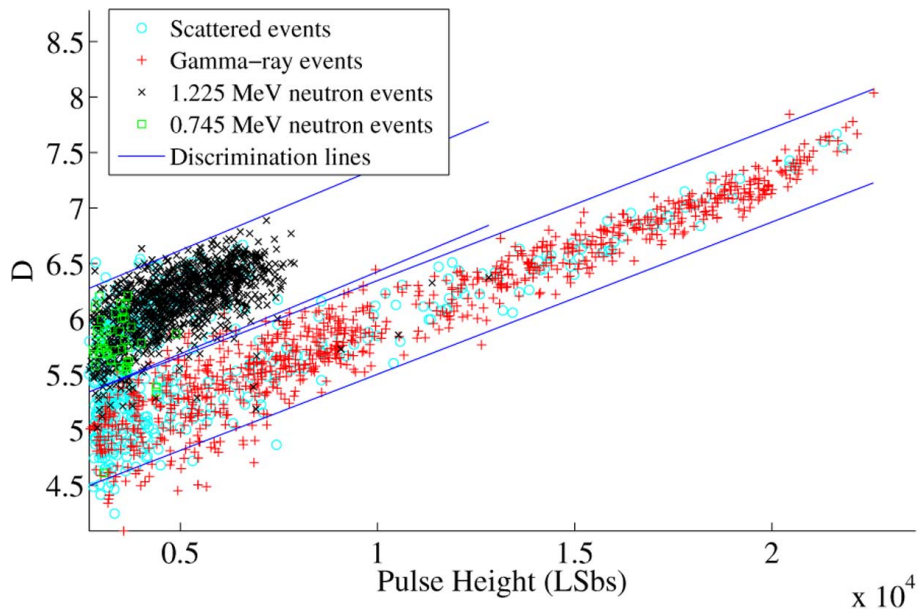

Fig. 6. The SDCC discrimination plane at a sampling rate of 250 $\mathrm{MSa} \cdot \mathrm{s}^{-1}$ together with the tag from the TOF discrimination corresponding to colour as per the legend.

TOF is not always available to an instrument in a mixed field environment. Therefore, to measure the efficacy of the SDCC method without TOF information the SDCC algorithm has been applied again to the 2500 pulses with the TOF data removed. In this application of the method, if a discrimination point lay between the gamma-line boundaries described above, then it was tagged as a gamma pulse. If the point lay between the neutron-line boundaries then it was tagged as a neutron. If the point did not lie between these two bands then the pulse is rejected and not included in any ratio calculation.

Fig. 5 is the discrimination plane with a sampling rate of 8 $\mathrm{GSa} \cdot \mathrm{s}^{-1}$ with the boundary method of pulse categorization. All 2500 pulses are categorized as neutrons or gamma rays to simulate the absence of TOF information.

The neutron and gamma-ray ratios are presented in Table II.

The MATLAB® scripts available to perform the PGA discrimination method during this research were only capable of operating at 250 $\mathrm{MSa} \cdot \mathrm{s}^{-1}$. For comparison, the SDCC method was re-evaluated at this reduced sampling rate. Fig. 6 shows the SDCC discrimination plane at 250 $\mathrm{MSa} \cdot \mathrm{s}^{-1}$ with the TOF tagging and Fig. 7 shows the discrimination plane with the boundary line tagging. Table I contains the data for the least-squares fits and Table II contains the data for the neutron-to-gamma ratios. Fig. 8 shows the discrimination plane for the PGA method.

A. FOM Calculation

To calculate the FOM for the SDCC and PGA methods arbitrary lines are needed from which to calculate a difference for each point so that the distribution over the plane can be obtained.

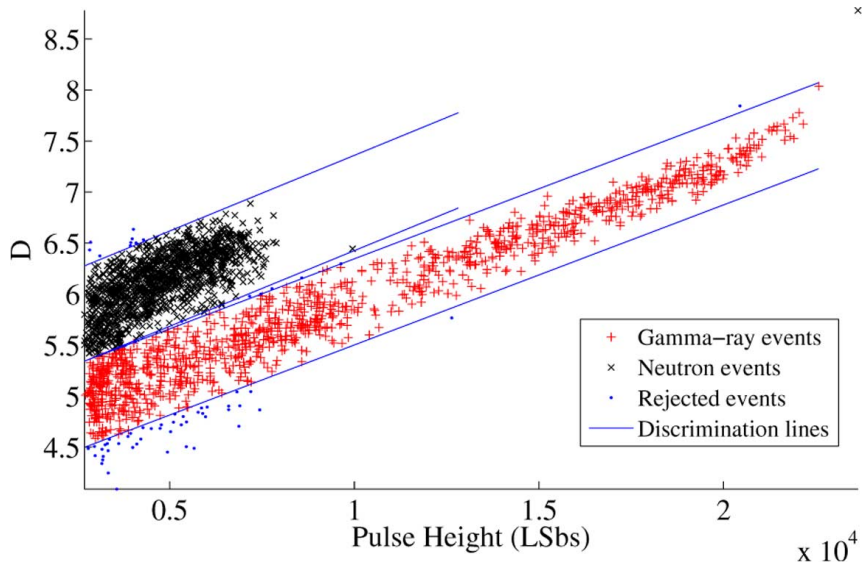

Fig. 7. The SDCC discrimination plane at a sampling rate of 250 $\mathrm{MSa \cdot s^{-1}}$ with the boundary method of pulse categorization.

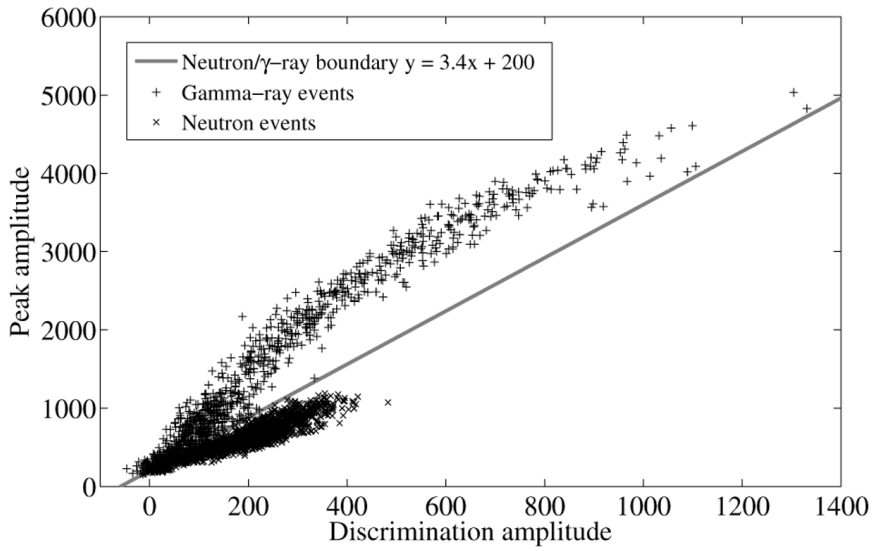

Fig. 8. The PGA discrimination plane at a sampling rate of 250 $\mathrm{MSa \cdot s^{-1}}$. The line in this figure is the discrimination line for the PGA method taken from [1].

TABLE II
THE NEUTRON AND GAMMA-RAY RATIOS FOR THE TOF, SDCC AND PGA DISCRIMINATION METHODS

Method	Neutrons	Gamma	Scatter or Rejected	Neutron/ Gamma
TOF	0.45	0.35	0.20	1.28
Uncertainty	±0.01	±0.01	±0.01	±0.07
SDCC at 8 GSa·s^{-1}	0.51	0.46	0.03	1.10
Uncertainty	±0.01	±0.01	±0.003	±0.03
SDCC at 250 MSa·s^{-1}	0.51	0.46	0.03	1.10
Uncertainty	±0.01	±0.01	±0.003	±0.03
PGA at 250 MSa·s^{-1}	0.61	0.39	-	1.57
Uncertainty	±0.02	±0.01	-	±0.06

For the PGA method this line was taken as the discrimination line given in Fig. 8. For the SDCC method the mean line between the gamma-ray and neutron centroid fits was taken as the corresponding threshold.

Fig. 9 shows the normalized distribution for the SDCC discrimination plane at the sampling rate of 8 $\mathrm{GSa \cdot s^{-1}}$ together with the double Gaussian fit. Fig. 10 shows the same distribution for the SDCC at a sampling rate of 250 $\mathrm{MSa \cdot s^{-1}}$ and Fig. 11 shows the PGA method's distribution.

Table III shows the coefficients gained from a non-linear least-squares fitting algorithm. With these coefficients we are able to calculate the FOM and these calculations are shown in Table IV.

The FOM has not been calculated for the discrimination planes with the boundary method of tagging events. The boundary method removes events on the very outskirts of the Gaussian distribution making the new distribution

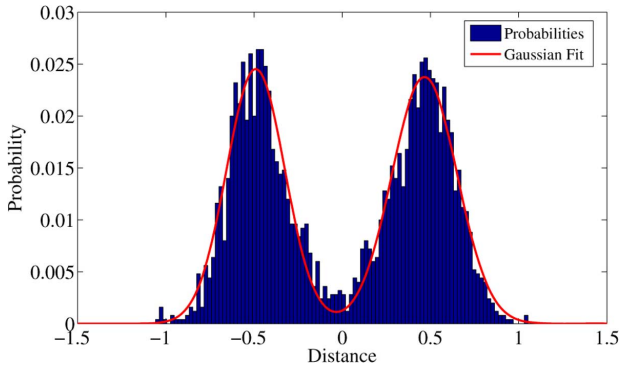

Fig. 9. The distribution of the distance from the mean line between the centroids (of the neutron and gamma plumes) and each point in the SDCC discrimination plane at 8 $\mathrm{GSa} \cdot \mathrm{s}^{-1}$.

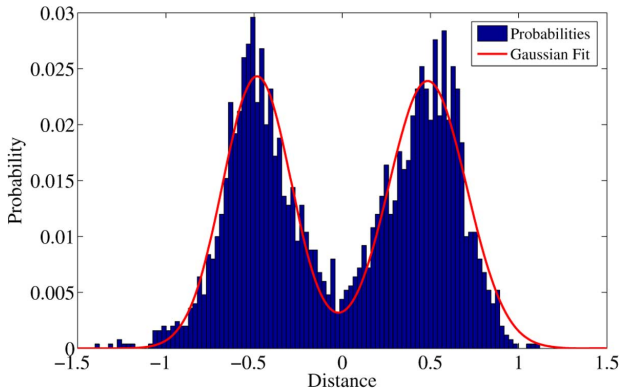

Fig. 10. The distribution of the distance from the mean line between the centroids (of the neutron and gamma plumes) and each point in the SDCC discrimination plane at 250 $\mathrm{MSa} \cdot \mathrm{s}^{-1}$.

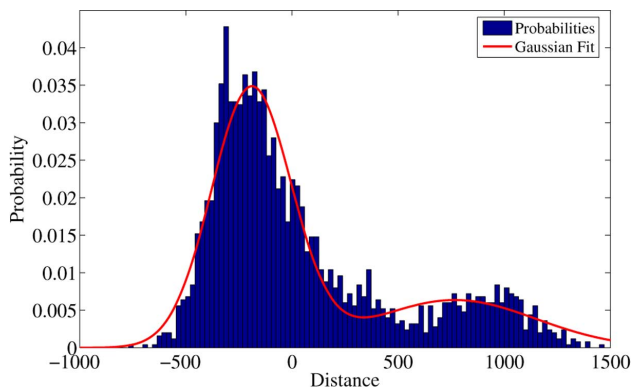

Fig. 11. The distribution of the distance from the discrimination line given in Fig. 8 and each point in the PGA discrimination plane at 250 $\mathrm{MSa} \cdot \mathrm{s}^{-1}$.

non-Gaussian. However, as only the outlying points are removed, the FWHM and the means of the two peaks will be unchanged and the FOM will therefore also be unchanged.

VI. Discussion

The discrimination planes for the SDCC method of discrimination presented in Figs. 4 and 6 suggest visually that the SDCC is a viable discrimination method. The TOF tags contained in these plots are grouped together well in the plane. The FOM figures in Table IV and the neutron to gamma ratios presented in Table II corroborate this suggestion. Furthermore, comparing

TABLE III
Coefficients From the Double Gaussian Fit Including Uncertainties

Method	A_1	μ_1	σ_1	A_2	μ_2	σ_2
SDCC at 8 GSa·s^{-1}	2.45 x10^{-2}	-0.491	0.112	2.38 x10^{-2}	0.466	0.131
Uncertainty	±6.94 x10^{-4}	±5.46 x10^{-3}	±3.85 x10^{-3}	±6.53 x10^{-4}	±5.92 x10^{-3}	±4.18 x10^{-3}
SDCC at 250 MSa·s^{-1}	2.43 x10^{-2}	-0.483	0.138	2.39 x10^{-2}	0.484	0.156
Uncertainty	±7.96 x10^{-4}	±7.40 x10^{-3}	±5.31 x10^{-3}	±7.50 x10^{-4}	±8.01 x10^{-3}	±5.77 x10^{-3}
PGA	3.46 x10^{-2}	-191	133	6.36 x10^{-3}	767	270
Uncertainty	±8.42 x10^{-4}	±5.87	±4.16	±6.15 x10^{-4}	±46.1	±40

TABLE IV
Figures of Merit Calculated With the Coefficients From Table III

Method	SDCC at 8 GSa·s^{-1}	SDCC at 250 MSa·s^{-1}	PGA
FOM	1.64	1.40	1.01
Uncertainty	±0.06	±0.03	±0.12

the FOM figures in Table III, the SDCC method appears to be an improvement over PGA method it terms of its discrimination capabilities.

The PGA algorithms used in this research use a 21-point finite impulse response (FIR) filter [1]. At 250 $\mathrm{MSa} \cdot \mathrm{s}^{-1}$ this corresponds to at least an 84 ns lag in system output before reaching a decision on pulse type. The SDCC method developed in this research uses no such filter and only processes samples 64 ns into the pulse after the peak. Due to this reduction in latency and also because of the reduction in complexity, the SDCC algorithm is an optimization over the PGA algorithm in terms of deployment on an embedded system.

The calculation of the linear least-squared fits used to generate the discrimination boundary lines in Figs. 5 and 7 is heavily reliant on the TOF tagging. This TOF data would not be available to any instrument designed to run as a portable embedded system. However, this research suggests that if that portable instrument had the capacity to be calibrated using TOF data then the boundary lines could be used again to discriminate neutrons between energies of 0.745 MeV and 1.225 MeV. Whether or not the straight line fits continue to perform as they did in this research in other environments and with different neutron energies is the subject of further research.

Inspection of Fig. 8 shows that the PGA method of discrimination for the dataset used in this research relies on one discrimination line. The gamma-ray and the neutron plumes merge together as the maximum height of the pulse decreases and the confidence in being able to discriminate decreases.

The SDCC method uses the centroids of the two separate plumes to calculate discriminating boundaries. In this research the boundary lines were set as $1.96\sigma_{perp}$ to account for 95% of

all events so that the number of rejected pulses were kept to a minimum. In the case of the 250 $\mathrm{MSa} \cdot \mathrm{s}^{-1}$ SDCC discrimination plane, presented in Fig. 7, this proved to be right at the limit of confidence for discrimination. If a bigger boundary between neutron and gamma-ray points in the plane is required for a measurement, then this can be achieved with a decrease in the multiplication factor of σ_{perp} corresponding to an increase in the likelihood of a pulse being rejected.

ACKNOWLEDGMENT

The authors would like to acknowledge the support of Lancaster University and in particular the Faculty of Science and Technology. They would also like to thank G. Taylor, N. Hawkes and D. Thomas at the National Physical Laboratory (NPL) Neutron Irradiation Facility who helped make this research possible.

David Shippen, the lead author on this research, died very suddenly shortly after the preparation of this article. David was in the second year of his Ph.D. and showed exceptional promise as a researcher in the field of nuclear science. He will be sadly missed by his family and colleagues.

REFERENCES

[1] M. D. Aspinall *et al.*, "Verification of the digital discrimination of neutrons and gamma rays using pulse gradient analysis by digital measurement of time of flight," *Nucl. Instrum. Meth. Phys. Res. A*, vol. 583, pp. 432–438, 2007.

[2] G. F. Knoll, *Radiation Detection and Measurement*, 3 ed. New York: Wiley, ch. 8.

[3] S. Marrone *et al.*, "Pulse shape analysis of liquid scintillators for neutron studies," *Nucl. Instrum. Meth. Phys. Res. A*, vol. 490, pp. 299–307, 2002.

[4] B. D'Mellow *et al.*, "Digital discrimination of neutrons and gamma-rays in liquid scintillators using pulse gradient analysis," *Nucl. Instrum. Meth. Phys. Res. A*, vol. 578, pp. 191–197, 2007.

[5] O. Rioul and P. Duhamel, "Fast algorithms for discrete and continuous wavelet transforms," *IEEE Trans. Inf. Theory*, vol. 38, pt. 2, pp. 569–586, 1992.

[6] L. Chongchun, L. Yaohui, Q. Zhingding, and D. Xiyu, "On the initialization of the discrete wavelet transform," in *Proc. IEEE Int. Conf. Intel. Process. Syst.*, Oct. 28–31, 1997, vol. 2, pp. 1220–1222.

[7] S. Arivazhagan, W. S. L. Jeberani, and G. Kumaran, "Performance comparison of discrete wavelet transform and dual tree discrete wavelet transform for automatic airborne target detection," in *Proc. Int. Conf. Compu. Intell. Multimedia Appl.*, Dec. 13–15, 2007, vol. 3, pp. 495–500.

[8] H. O. Mota, F. H. Vasconcelos, and R. M. da Silva, "Real time wavelet transform algorithms for the processing of continuous streams of data," in *Proc. IEEE Int. Workshop Intell. Signal Process.*, Sep. 1–3, 2005, pp. 346–351.

[9] M. A. Farahani and M. Eshghi, "Architecture of a wavelet packet transform using parallel filters," in *Proc. 2006 IEEE Region 10 Conf. TENCON*, Nov. 14–17, 2006, pp. 1–4.

[10] A. Jensen and A. la Cour-Harbo, *Ripples in Mathematics, the Discrete Wavelet Transform*. New York: Springer, pp. 62–62.

[11] M. D. Aspinall *et al.*, "The empirical characterization of organic liquid scintillation detectors by the normalized average of digitized pulse shapes," *Nucl. Instrum. Meth. Phys. Res. A*, vol. 578, pp. 261–266, 2007.

[12] P. R. Bevington and D. K. Robinson, *Data Reduction and Error Analysis for the Physical Sciences*, 3 ed. New York: McGraw Hill, pp. 102–102.